Redox Biology 14 (2018) 645–655

Contents lists available at ScienceDirect

Redox Biology

journal homepage: www.elsevier.com/locate/redox

Oxidative stress-driven pulmonary inflammation and fibrosis in a mouse model of human ataxia-telangiectasia

Ruth Duecker[a,*], Patrick Baer[b], Olaf Eickmeier[a], Maja Strecker[a], Jennifer Kurz[a], Alexander Schaible[c], Dirk Henrich[c], Stefan Zielen[a], Ralf Schubert[a]

[a] Division for Allergy, Pneumology and Cystic Fibrosis, Department for Children and Adolescence, Goethe-University, Frankfurt/Main, Germany
[b] Division of Nephrology, Department of Internal Medicine III, Goethe-University, Frankfurt/Main, Germany
[c] Department of Trauma, Hand & Reconstructive Surgery, Goethe-University, Frankfurt/Main, Germany

ARTICLE INFO

Keywords:
Pulmonary inflammation
Lung fibrosis
Mice
Oxidative stress

ABSTRACT

Lung failure is responsible for significant morbidity and is a frequent cause of death in ataxia-telangiectasia (A-T). Disturbance in the redox balance of alveolar epithelial cells must be considered as a causal factor for respiratory disease in A-T. To investigate bronchoalveolar sensitivity to reactive oxygen species (ROS) and ROS-induced DNA damage, we used bleomycin (BLM) to induce experimental inflammation and fibrotic changes in the *Atm*-deficient mouse model.

BLM or saline was administered by oropharyngeal instillation into the lung of *Atm*-deficient mice and wild-type mice. Mice underwent pulmonary function testing at days 0, 9, and 28, and bronchoalveolar lavage (BAL) was analysed for cell distribution and cytokines. Lung tissue was analysed by histochemistry.

BLM administration resulted in a tremendous increase in lung inflammation and fibrotic changes in the lung tissue of *Atm*-deficient mice and was accompanied by irreversible deterioration of lung function. ATM (ataxia telangiectasia mutated) deficiency resulted in reduced cell viability, a delay in the resolution of γH2AX expression and a significant increase in intracellular ROS in pulmonary epithelial cells after BLM treatment. This was confirmed in the human epithelial cell line A549 treated with the ATM-kinase inhibitor KU55933.

Our results demonstrate high bronchoalveolar sensitivity to ROS and ROS-induced DNA damage in the *Atm*-deficient mouse model and support the hypothesis that ATM plays a pivotal role in the control of oxidative stress-driven lung inflammation and fibrosis.

1. Introduction

Ataxia-telangiectasia (A-T) is a rare autosomal recessive disorder caused by mutations in the ataxia-telangiectasia mutated (ATM) gene that results in the defective repair of DNA double-strand breaks. The clinical phenotype is characterised by progressive neurodegeneration, immunodeficiency, elevated risk of malignancies and a high rate of respiratory failure [1,2]. Mortality is generally due to respiratory diseases, which are a frequent cause of death in patients with A-T [3]. Primary symptoms include recurrent respiratory tract infections and bronchiectasis, aspiration and respiratory muscle abnormalities, as well as interstitial lung disease and pulmonary fibrosis [4–6].

It has been proposed that ongoing low-grade inflammation and oxidative stress might be an underlying mechanism leading to the clinical pathogenesis of A-T [7–9]. McGrath-Morrow et al. demonstrated that elevated serum IL-8 and IL-6 levels in A-T patients were found to be associated with lower lung function parameters [7,8]. Elevated IL-6 and IL-8 have also been described for other lung diseases, such as cystic fibrosis and chronic obstructive pulmonary disease (COPD), which both have serum and sputum cytokine profiles associated with their pathologic conditions [10–12]. In addition to inflammation, there is a growing body of evidence that reactive oxygen species (ROS) are involved in pulmonary disease in A-T. Barlow et al. showed that a loss of the ATM protein causes oxidative damage in target organs in *Atm*-deficient mice [13]. In addition, increased ROS and reduced anti-oxidative capacity were demonstrated in serum from patients with A-T [14,15]. A recent study from our group revealed a significantly higher amount of oxidative DNA damage based on analysis of 8-hydroxy-2′-deoxyguanosine (8-OH-dG) in the bronchial lavage fluid (BALF) of *Atm*-deficient mice compared to wild-type animals [9]. The use of antioxidants has been shown to reduce oxidative stress, increase lifespan and correct neurobehavioural deficits in these mice [16,17].

As first, Eickmeier et al. induced lung inflammation in *Atm*-deficient

* Correspondence to: Department for Children and Adolescence Goethe University, Theodor-Stern-Kai 7, 60590 Frankfurt/Main, Germany.
E-mail address: RuthPia.Duecker@kgu.de (R. Duecker).

https://doi.org/10.1016/j.redox.2017.11.006
Received 1 August 2017; Received in revised form 13 October 2017; Accepted 7 November 2017
Available online 10 November 2017

mice by using an acute lung injury model [18]. The data indicated that restricted lung function and a high sensitivity to hydrochloric acid induced inflammation in these mice. However, this short-term model did not analyse the role of ROS in pulmonary inflammation, and fibrotic changes in the lung tissue were not investigated. To take a closer look at the role of ROS-induced inflammation and fibrotic changes in respiratory disease in A-T, we used the bleomycin (BLM) model, which is widely used in rodents to induce pulmonary fibrosis [19]. BLM is a chemotherapeutic antibiotic produced by the bacterium *Streptomyces verticillus* that plays an important role in the treatment of different cancer types [20,21]. Pulmonary side effects of BLM treatment are the induction of single- and double-strand DNA breaks by the chelation of metal ions and the generation of superoxide and hyperoxide free radicals [22].

Revealing the origin of A-T lung disease and its progression may help in the discovery and development of new therapeutic interventions. Therefore, the aim of the present study was to investigate bronchoalveolar sensitivity to ROS and ROS-induced DNA damage using the pulmonary bleomycin model in the *Atm*-deficient mouse.

2. Materials and methods

2.1. Animals

Atm-deficient mice (Atmtm1Awb; 8–10 weeks old), in a 129SvEv background, were used as the animal model. The animal studies were performed according to the protocols approved by the German Animal Subjects Committee (Gen. Nr. FK/1001). Mice were housed in plastic cages on a 12-h light/12-h dark cycle with access to food and water ad libitum until harvest. Weight was taken every single day (0 − 28) throughout the treatment. All surgery was performed under ketamine/xylazine anaesthesia (20% ketamine, CuraMED GmbH, Karlsruhe, Germany; 8% xylazine, Bayer Vital GmbH, Leverkusen, Germany), and every effort was made to minimise suffering.

2.2. Bleomycin model

Bleomycin sulphate (Sigma-Aldrich, Germany) was dissolved in sterile 0.9% saline and administered as a single dose of 0.75 mg/kg body weight (a dose chosen based on our data from a preliminary dosage experiment, data not shown) by oropharyngeal instillation into the lung of lightly anaesthetised (2.0% Isoflurane, Abbott GmbH, Germany) *Atm*-deficient mice and wild-type mice on day 0. Control animals received a body weight adjusted dose of saline alone. Oropharyngeal aspiration (OA) was performed as described by De Vooght et al. [23]. Briefly, mice were held vertically, the tongue was pulled out with forceps, and the fluid was placed onto the distal part of the oropharynx while the nose was gently closed. Bronchoalveolar lavage, pulmonary function tests and perfusion were performed and lung tissue was harvested at day 0, 9 and 28 post-dosing.

2.3. Cell Culture

A549 cells were cultured in Dulbecco's modified Eagle's medium (DMEM) supplemented with 2 mM L-glutamine, 1% v/v penicillin/streptomycin (Gibco by Life Technologies, Germany) and 10% v/v foetal bovine serum (FBS) (Sigma-Aldrich, Germany) [24]. Proliferative cultures were incubated at 37 °C in a humidified, 5% CO_2 incubator, and subculture was carried out by washing the cell monolayers twice with calcium and magnesium-free phosphate-buffered saline (PBS) followed by the addition of 0.25% trypsin/EDTA solution (Life Technologies, Germany) and incubation at 37 °C until the cells detached. Trypsin was inactivated by the addition of growth medium before seeding into fresh T25 flasks at densities of 2–4 $\times 10^4$ cells/cm ^{2}. The medium was changed every 2–4 days. The passages used for the following experiments were 6–12.

The murine alveolar epithelial cells and the human alveolar epithelial cell line A549 were stimulated with 100 mU bleomycin sulphate (Calbiochem, Germany) for 24 h. Additionally, A549 cells were incubated with the ATM-kinase inhibitor, 10 μM KU55933 (Selleckchem, Germany) 1 h prior to BLM stimulation.

2.4. Primary murine alveolar epithelial cells

The isolation of primary, whole lung cells was performed as described by Corti et al. [25]. Briefly, mice were sacrificed by CO_2 asphyxiation, the thorax was removed, and the diaphragm was carefully punctured and removed to expose the heart. The right ventricle was perforated with a 26 G cannula and perfused with a 20 mL syringe filled with cold phosphate-buffered saline (PBS) until free of blood. To expose the trachea, the salivary glands were removed, and a 22 G cannula was inserted into the trachea and fixed with thread around the trachea and the catheter. A total of 1.5 mL of dispase (Corning, USA; pre-warmed to 37 °C) was carefully instilled into the lung so that all the lobes were fully expanded. After that, 0.5 mL of 1% low-melt agarose (Bio&Sell, Germany) was also instilled into the lung. Backflow was avoided by leaving the syringe on the catheter. After cutting the trachea, the lung, heart and thymus were removed, and the lung was incubated in 3 mL of dispase at room temperature for 45 mins on a bench rocker. Lung tissue was minced using the gentleMACS Dissociator (Miltenyi Biotec, Bergisch-Gladbach, Germany) according to the manufacturer's protocol with 3 mL of gentle MACS Buffer (5 mL DMEM, 100 U/mL penicillin, 100 μg/mL streptomycin, 2 mM glutamine, 20 mM HEPES, 120 U DNase). For further cell proliferation assays (XTT assay), 2.5 $\times$ 10^4 cells were used, and 2 $\times$ 10^5 cells were used for FACS analysis.

2.5. Flow cytometry

The expression of specific cell surface markers on primary pulmonary epithelial cells was determined using a BD FACSVerse cytometer (Beckman Coulter, Inc., CA, USA). Cell suspensions were transferred to FACS tubes and washed twice with phosphate-buffered saline (PBS; Life Technologies, Darmstadt, Germany). Then, 0.2 $\times$ 10^6 cells in 100 μL of PBS were blocked with CD16/32 for 10 min, and the surface was stained for 20 min in the dark with the following antibodies: SPC-FITC, CD45-PE, CD326-PECy7, CD31-APC, Sca-1-FITC, CD11c-PECy7 (BD Bioscience, San Jose, USA). After a washing step, 300 μL of PBS was added, and the samples were measured. FACSuite Software was used to analyse the data.

2.6. XTT assay (Supplement)

Viability was measured in A549 cells and primary murine AEC2 cells via the XTT assay. Cells were then seeded in 96-well plates at a specified density (A549 25,000 cells/well, AEC2 5 $\times$ 10^4 cells/well) and were incubated with different concentrations (1 mU, 10 mU and 100 mU) of bleomycin sulphate (Calbiochem, Germany). Ethanol (70%) served as the positive control. The XTT solution (Applichem, Germany) was added, and the cells were incubated further for 4 h at 37 °C and colorimetrically quantified (absorbance 450 nm, reference 630 nm).

2.7. Reactive oxygen species (ROS)

A549 cells or whole-lung cells, isolated from 6 to 8-week-old *Atm*-deficient and wild-type mice (2 $\times$ 10^5), were untreated or treated with 100 μM bleomycin for 24 h, collected and suspended in 1 mL PBS containing 5 μM DCF-DA (2′, 7′ –dichlorofluorescein diacetate, Molecular Probes, Inc., OR, USA) for 15 min. Additionally, murine cells were surface-stained with αCD326-PE-Cy7 (BD Bioscience, San Jose, USA), αSPC-APC (Bioss, USA) and αSca-1-PE (Biolegend, San Diego, USA) and analysed by flow cytometry on a BD FACSVerse cytometer (Beckman Coulter, Inc., CA, USA) using the BD FACSuite Software. The

FITC signals from DCF in live cells were determined for SPC^+ and $CD326^-Sca\text{-}1^+$ cells.

After collection and a washing step, the cells were incubated with 5 μM DCF-DA for 15 min 100 μM H_2O_2 for 30 min served as positive control.

2.8. Comet assay

A549 cells were seeded onto 24-well cell culture plates at a density of 2×10^5 cells/well. The following day, cells were incubated with or without 10 μM KU55933 1 h prior BLM-stimulation [10 mU] for 3 h at 37 °C. OxiSelect™ Comet Assay Kit (Cell Biolabs, Inc., San Diego, USA) was used to assess for DNA damage following the manufacturer's protocol. After staining with Vista Green DNA dye solution, samples were examined and photographed by fluorescent microscopy at 100x magnification (Zeiss, Germany). Tail length was determined as the distance between the edge of the nucleus and the end of the tail. A minimum of 50 determinations per sample was made during data analysis.

2.9. γH2AX assay

Whole-lung cells isolated from *Atm*-deficient and wild-type mice or A549 cells, incubated with the ATM-kinase inhibitor 1 h prior BLM-stimulation (100 mU, 0 h, 3 h, 24 h, 48 h and 72 h), were used for γH2AX analysis. It was performed as described by Tanaka et al. [26] with slight modification. Briefly, after the BLM treatment cell suspensions were centrifuged, and the supernatants were removed. The remaining cell pellet was fixed with 100 μL BD Cytofix™ fixation buffer for 10 min at room temperature (RT). After a washing step, the cells were permeabilised using 100 μL ice-cold BD™ Phosflow Perm Buffer III and incubated for 5 min at RT. Cells were washed with PBS twice and blocked with 3% foetal calf serum in PBS for 30 min at RT. The anti-H2AX (S139) antibody (Alexa Fluor 647 Mouse anti-H2AX(pSer139), BD Pharmingen) was added (1:10) and incubated for 60 min at RT in the dark. After washing the cells three times with PBS, the nuclei were counterstained with Hoechst33342 (5 μg/mL, green pseudocolour) before analysing the cells with a BD FACSVerse cytometer. The data were evaluated using FACSuite software. For the immunofluorescent staining, cells were seeded in chamber slides. After a 48 h culture, the cells were exposed to 100 mU bleomycin for 24 h. The cells were fixed, permeabilised and stained with 1:10 Alexa Fluor 488 Mouse anti-H2AX (PSer139) (BD Pharmingen). Cell nuclei were counterstained with DAPI (blue-fluorescent DNA stain).

2.10. Bronchoalveolar lavage fluid

Immediately after lung function analysis, bronchoalveolar lavage fluid (BALF) was obtained. The trachea was cannulated, and the lung lavage was obtained by washing 3 times with 1.0 mL of sterile PBS plus 0.6 mM EDTA. The lavage fluid was pooled and centrifuged at 3000 rpm for 10 min, and the cell pellet was resuspended in erythrocyte-lysing buffer. The lavage cells were then washed with sterile PBS, after which the total cell count was determined as previously described [18]. The resuspended cell pellets were then centrifuged in a cytocentrifuge (Thermo Scientific Shandon, Dreieich, Germany), and a differential leukocyte count was performed at a magnification of ×100 under light microscopy (Olympus, Hamburg, Germany) by counting 400 cells stained with Pappenheim-Giemsa.

2.11. Cytokines

To study inflammatory mediators after treatment with bleomycin *in vivo*, the pro-inflammatory cytokines IL-6, TNF-α and CXCL1/KC were analysed using the BD CBA Flex Sets (BD Biosciences-Pharmingen, USA). Frozen supernatants were thawed at room temperature and centrifuged at 10,000 rpm for 10 min at 4 °C. For this, 20 μL of Flex Set Standards (0.274 − 200 pg/mL) and samples (50 μL) were incubated with 20 μL of capture bead mixture, 20 μL of mouse detection reagent and 100 μL of enhanced sensitivity detection reagent in 96-well plates at room temperature in the dark for 1 h. After washing, samples were measured with a BD FACS Array™ cytometer (BD Bioscience-Pharmingen, USA). FCAP Array Software (BD Bioscience-Pharmingen, USA) was used to analyse the data.

2.12. Pulmonary function

Atm-deficient mice and wild-type mice underwent pulmonary function testing using a computer-controlled piston ventilator (flexiVent, SCIREQ Inc., Montreal, Canada) before, 9 days and 28 days after treatment. Briefly, mice were anaesthetised, a tracheotomy was performed, and the trachea was cannulated. Then, the mice were placed on a temperature controlled heat blanket, the trachea was exposed, and the previously calibrated cannula (1.2 cm, 18 gauges) was inserted and fixed using a suture. Ventilation was maintained at a rate of 150 breaths/min, a tidal volume of 10 mL/kg, and a positive end-expiratory pressure of 3 cm of water. Mice were allowed to acclimate to the ventilator for 2–3 min before measurement.

Lung function parameters were calculated by fitting pressure and volume data to the single compartment model, by measuring respiratory system resistance (Rrs), dynamic compliance (Crs) and elastance (Ers), and by analysing with flexiWare 7 Software.

2.13. Histological examination

After BAL, the left main bronchus was clamped, and the left lung was excised for further RNA examination. The right lung of animals from each experimental group was fixed in 4% paraformaldehyde at 20–25 cm H_2O inflation pressure, embedded in paraffin and cut into 2–4 μm thick sections. Mouse lung sections were stained with haematoxylin and eosin (H&E, Roth, Germany) or Masson's trichrome (Polysciences Europe GmbH, Germany) in accord with the manufacturer's specifications. For inflammatory cell count, the tissue specimen was evaluated for macrophages, neutrophils and lymphocytes at a magnification of ×50 or ×100 by light microscopy (Zeiss, Germany).

The severity of fibrosis was assessed by light microscopy, and the Ashcroft scale was used for the semi-quantitative histological analysis of the fibrotic changes induced by BLM. The degree of fibrosis in each lung section was assigned a mean fibrotic severity score from 0 (normal) to 8 (total fibrosis of the field), and an average was obtained for each slide [27]. Thirteen observers, blinded to the experimental groups, were randomly assigned to evaluate photographs of fibrotic lung sections. They were provided with a description of the scale and sample photographs by the authors to assist in evaluation. Special attention was paid to infiltration of inflammatory cells, thickening of alveolar walls and collagen deposition.

2.14. Statistics

Statistical analyses were performed using GraphPad Prism 5.0 (GraphPad Software, San Diego, CA, USA). Values are presented as the means (± SEM) and were analysed using a Mann-Whitney *U*-test or a Wilcoxon-Mann-Whitney test. For multiple comparisons, we used Kruskal-Wallis testing. $P < 0.05$ was regarded as significant.

3. Results

3.1. No differences in cell subsets and pro-inflammatory cytokines in the BALF of untreated Atm-deficient mice and wild-type littermates

As shown before by Eickmeier et al. [18], the total cell number, cell subsets, and pro-inflammatory cytokines in the bronchoalveolar lavage fluid (BALF) of untreated *Atm*-deficient mice compared to their wild-

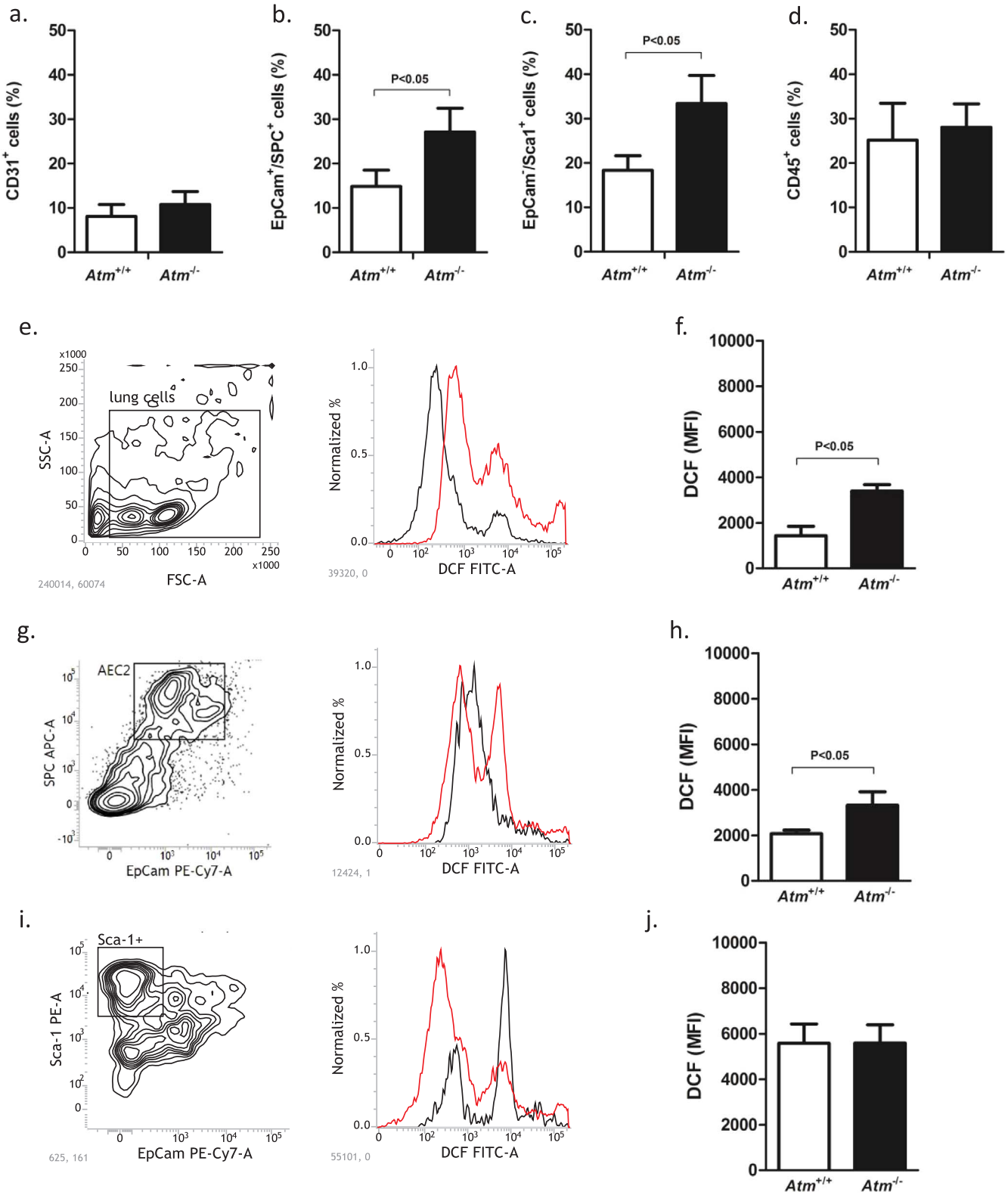

Fig. 1. Analysis of primary whole-lung cells from *Atm*-deficient ($Atm^{-/-}$, n = 5) and wild-type mice ($Atm^{+/+}$, n = 5). Cells were isolated and surface stained for (a) endothelial cells ($CD31^+$), (b) epithelial cells ($EpCam^+/SPC^+$), (c) fibroblasts ($CD326^-/Sca1^+$, and (d) haematopoietic cells ($CD45^+$) and analysed by flow cytometry. Measurement of ROS in untreated primary whole-lung cells, alveolar type II (AEC2) and Sca-1^+ mesenchymal cells isolated from $Atm^{-/-}$ and $Atm^{+/+}$ mice. Representative contour plots of (e) primary whole-lung cells, (g) AEC2 and (i) Sca-1^+ cells and corresponding FACS histogram of the $Atm^{+/+}$ (black) versus $Atm^{-/-}$ (red) ROS levels incubated with 5 μM DCF. Combined MFI data are presented in f, h and j. Data are expressed as the mean ± SEM. * $P^{<}0.05$. BLM = bleomycin, DCF = 2′,7′ –dichlorofluorescein diacetate, MFI = mean fluorescence intensity, ROS = reactive oxygen species.

type littermates were determined. There were no significant differences in the percentage of macrophages, neutrophils and lymphocytes in BALF of untreated *Atm*-deficient compared to wild-type mice (Supplementary Fig. 1 a-c). The levels of the pro-inflammatory cytokines IL-1β, IL-6 and TNF-α revealed no significant difference between the two genotypes (Supplementary Fig. 1 d-f).

3.2. Increase in alveolar epithelial type II cells and fibroblasts in Atm-deficient mice

Characterisation of primary lung cells isolated from untreated *Atm*-deficient mice and wild-type littermates showed a significantly increased percentage of SPC and CD326 double-positive, surfactant-producing alveolar epithelial type 2 cells (AEC2) and Sca-1 positive CD326 negative fibroblasts in *Atm*-deficient mice (AEC2: 27.07% ± 5.4, $P < 0.05$; fibroblasts: 33.37% ± 6.31, $P < 0.05$) compared to wild-type mice (AEC2: 14.83% ± 3.68; fibroblasts: 18.33% ± 3.31) (Fig. 1b, c). There were no significant differences in the percentage of $CD31^+$ endothelial and $CD45^+$ haematopoietic cells in the lungs of *Atm*-deficient mice compared to wild-type mice (Fig. 1a, d).

3.3. Increased ROS in AEC2 from Atm-deficient mice

We measured ROS in primary lung cells isolated from *Atm*-deficient and healthy control mice by DCF staining and flow cytometry. DCF fluorescence was significantly increased in untreated primary lung cells from *Atm*-deficient mice relative to wild-type mice ($Atm^{-/-}$ 3399 MFI ± 4.38; $Atm^{+/+}$ 1440 MFI ± 5.23, $P < 0.05$) (Fig. 1e, f), especially in AEC2 ($Atm^{-/-}$ 3322 MFI ± 6.36; $Atm^{+/+}$ 2072 MFI ± 4.42; $P < 0.05$) (Fig. 1g, h). Regarding the Sca-1 positive fibroblasts, there were no differences between *Atm*-deficient mice and healthy control mice ($Atm^{-/-}$ 5587 MFI ± 7.39; $Atm^{+/+}$ 5579 MFI ± 7.61) (Fig. 1i, j).

3.4. BLM strongly affects the body weight of Atm-deficient mice in vivo

To elucidate bronchoalveolar sensitivity to reactive oxygen species (ROS) and ROS-induced DNA damage, we used BLM to induce experimental inflammation and fibrotic changes in the *Atm*-deficient mouse model (Fig. 2a). Daily weight control confirmed previous findings that *Atm*-deficient mice exhibit lower body weight than their wild-type littermates (Fig. 2b). Although the pattern of weight change looks similar across the time course, we observed a longer period of significant weight loss in *Atm*-deficient mice from day 7 to day 10 (initial weight: 18.54 g ± 0.11; day 7: 17.20 g ± 0.17, $P < 0.01$; day 8: 16.66 g ± 0.10, $P < 0.001$; day 9: 16.69 g ± 0.15, $P < 0.01$, day 10: 17.23 g ± 0.59, $P < 0.01$) and at day 15 after BLM instillation (17.34 g ± 0.48, $P < 0.05$) whilst wild-type mice only show a significant weight reduction at day 7 (initial weight: 20.69 g ± 0.11, on day 9: 20.54 g ± 0.16; $P < 0.01$).

A direct comparison of the delta weight changes ($Atm^{-/-}$: −0.93 ± 0.48; $Atm^{+/+}$: 1.06 ± 0.50; $P < 0.001$) regarding body weight before treatment (day 0) and weight after treatment (day 28) resulted in a significant difference between the wild-type mice and *Atm*-deficient mouse cohort (Fig. 2c).

3.5. Tremendous increase in lung inflammation in Atm-deficient mice after BLM administration

To determine the effects of ATM on the host response to airway injury, BAL was performed before, 9 and 28 days after BLM instillation and pulmonary leukocyte numbers were obtained. As shown previously, there were no significant differences in total BALF cells, macrophages, neutrophils, lymphocytes, or in pro-inflammatory cytokines in *Atm*-deficient mice compared to wild-type mice before BLM application (Fig. 3a-g). After BLM application, total cell numbers, macrophages, neutrophils, and lymphocytes were significantly higher in *Atm*-deficient mice compared to wild-type mice (total cells: $Atm^{-/-}$ 118.65 $\times 10^3$ cells ± 15.85 $\times 10^3$, $Atm^{+/+}$ 52.67 $\times 10^3$ cells ± 8.12 $\times 10^3$, $P < 0.001$; macrophages: $Atm^{-/-}$ 83.35 $\times 10^3$ cells ± 7.63 $\times 10^3$, $Atm^{+/+}$ 49.11 $\times 10^3$ cells ± 7.24 $\times 10^3$, $P < 0.001$; neutrophils: $Atm^{-/-}$ 28.07 $\times 10^3$ cells ± 11.43 $\times 10^3$, $Atm^{+/+}$ 1.95 $\times 10^3$ cells ± 0.83 $\times 10^3$, $P < 0.01$; lymphocytes: $Atm^{-/-}$ 6.87 $\times 10^3$ cells ± 3.07 $\times 10^3$, $Atm^{+/+}$ 1.61 $\times 10^3$ cells ± 0.55 $\times 10^3$, $P < 0.05$). On day 28, we observed a decline in the number of inflammatory cells such as neutrophils and lymphocytes in both genotypes (Fig. 3a-d). BLM administration significantly increased levels of IL-6, TNF-α and CXCL1/KC in the BALF of

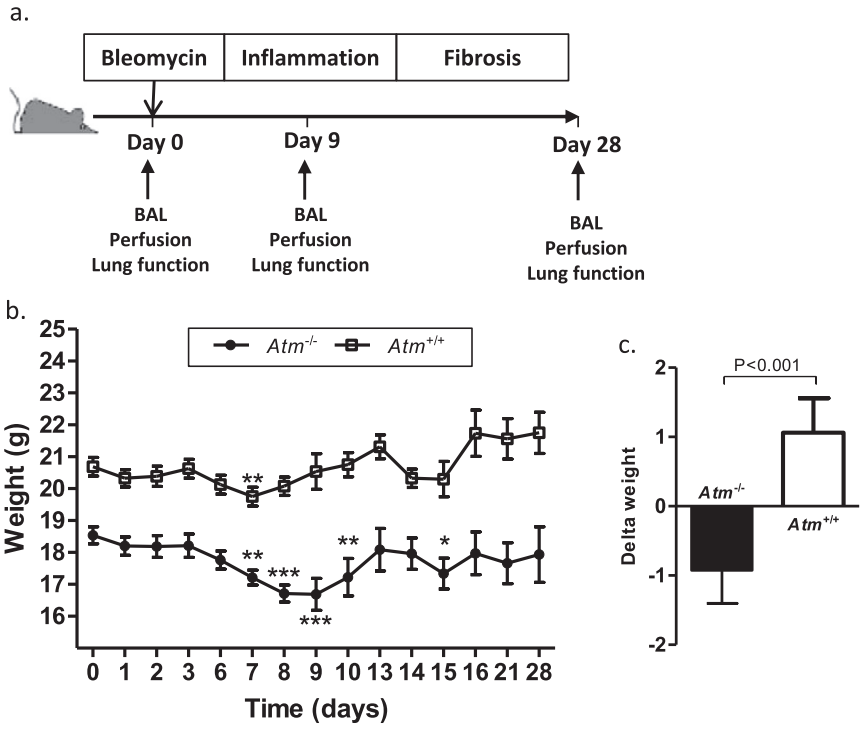

Fig. 2. Overview of the study design and effect of BLM instillation on weight gain in *Atm*-deficient mice (n ≥ 8) in comparison to wild-type mice (n ≥ 8). (a) 0.75 mg/kg body weight BLM or saline was given to $Atm^{-/-}$ mice or $Atm^{+/+}$ control groups via the oropharyngeal route on day 0. On days 9 and 28, lung function tests, BAL and perfusion were performed. (b) Measurement of the body weight of $Atm^{+/+}$ mice and $Atm^{-/-}$ mice at different time points (0–28 days) after BLM-induced lung injury. (c) Changes in body weights of $Atm^{+/+}$ and $Atm^{-/-}$ mice on day 0 compared to the end of the observation period (d28). Data are expressed as the mean ± SEM. * $P < 0.05$, ** $P < 0.01$, *** $P < 0.001$ compared to baseline. BAL = bronchoalveolar lavage, BLM = bleomycin.

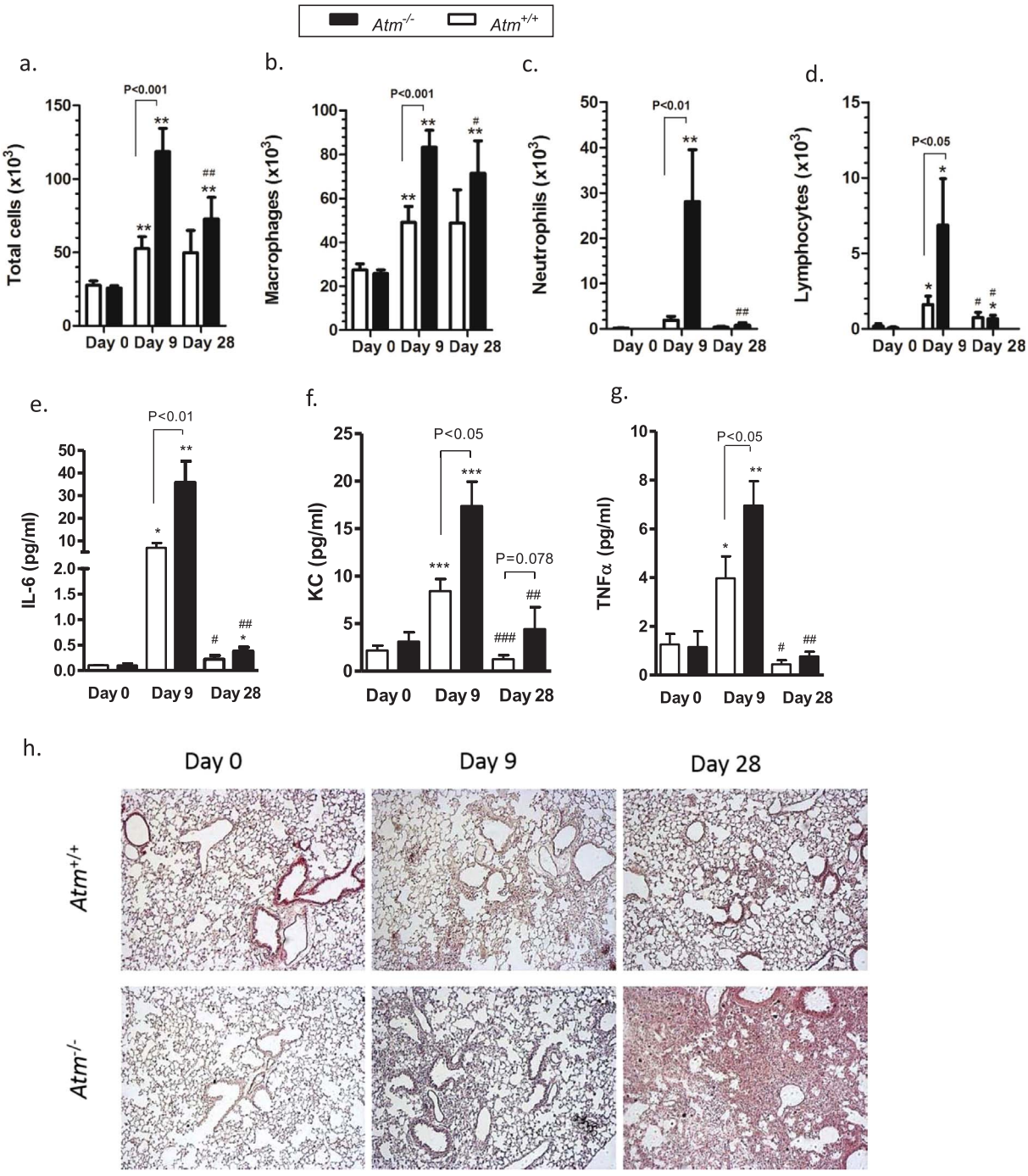

Fig. 3. Inflammation in *Atm*-deficient ($Atm^{-/-}$) and wild-type mice ($Atm^{+/+}$). (a) Total cells, (b-d) cell subsets and (e-g) cytometric bead analysis of pro-inflammatory cytokines (IL-6, CXLC1/KC and TNF-α) in bronchoalveolar lavage fluid (BALF) from $Atm^{-/-}$ and $Atm^{+/+}$ mice before or 9 and 28 days after BLM administration. (h) Representative histological lung sections at 0, 9 and 28 days after the oropharyngeal instillation of saline or BLM in $Atm^{-/-}$ and $Atm^{+/+}$ mice stained with haematoxylin and eosin. Data are expressed as the mean ± SEM. * compared to baseline, # compared $Atm^{-/-}$ vs. $Atm^{+/+}$, * $P < 0.05$, ** $P < 0.01$, # $P < 0.05$, ## $P < 0.01$. BLM = bleomycin.

Atm-deficient mice compared to wild-type mice (IL-6: $Atm^{-/-}$ 35.78 pg/mL ± 0.38, $Atm^{+/+}$ 6.89 pg/mL ± 0.21, $P < 0.01$; TNF-α: $Atm^{-/-}$ 6.96 pg/mL ± 0.12, $Atm^{+/+}$ 3.97 pg/mL ± 0.13, $P < 0.05$; KC: $Atm^{-/-}$ 17.39 pg/mL ± 0.15, $Atm^{+/+}$ 8.42 pg/mL ± 0.16, $P < 0.05$) on day 9. Up to 28 days after BLM instillation, we found a marked decline in IL-6, TNF-α and KC release in cells, without differences between the two genotypes (Fig. 3e-g).

3.6. BLM treated Atm-deficient mice demonstrate subpleural lung injury and fibrosis

To analyse the inflammatory and fibrogenic processes, we performed histological analysis with H&E (Fig. 3h) and Masson's Trichrome staining (Fig. 4a). Lung sections showed normal lung parenchyma with clear alveoli in lung sections from saline treated *Atm*-deficient and wild-type mice (day 0). On day 9, BLM-induced lung injury led to moderate infiltration of inflammatory cells, primarily neutrophils, and epithelial disruption as well as alveolar septal thickening in *Atm*-deficient mice relative to wild-type mice, and this injury then

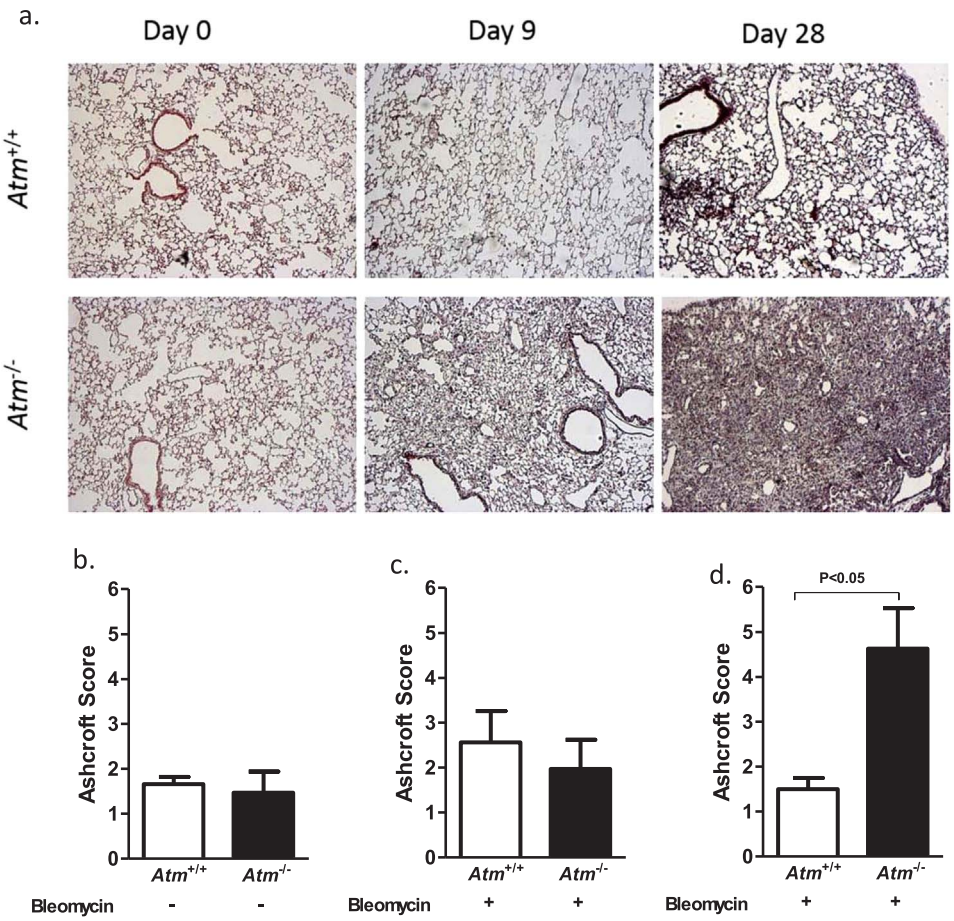

Fig. 4. Effect of BLM on collagen deposition in the lungs of *Atm*-deficient ($Atm^{-/-}$) and wild-type mice ($Atm^{+/+}$). (a) Representative histological findings with Masson's trichrome staining before, 9 and 28 days after BLM administration in $Atm^{-/-}$ compared to $Atm^{+/+}$ mice. Representative images at ×50 magnification. (b-d) Semi-quantitative analysis of stained lung sections using the Ashcroft fibrosis score on days 0, 9 and 28. Data are expressed as the mean ± SEM. * P<0.05. BLM = bleomycin.

resulted in profound thickening of lung interstitium and lung disruption 28 days after BLM instillation (Fig. 4a). Masson's Trichrome staining of the connective tissue demonstrated massive fibrotic changes in *Atm*-deficient mice after BLM administration. Ashcroft scoring, which scores the degree of fibrotic changes, revealed that this change is progressive in *Atm*-deficient mice and led to significantly higher scores at day 28 compared to wild-type mice ($Atm^{-/-}$ 4.63 ± 0.90, $Atm^{+/+}$ 1.5 ± 0.25, P < 0.05) (Fig. 4d.).

3.7. Atm-deficient mice show increased lung resistance and elastance and decreased compliance

To examine whether ATM deficiency influenced lung mechanics, we performed lung function testing before BLM application (day 0), 9 and 28 days after BLM instillation. Untreated *Atm*-deficient mice showed significantly increased lung resistance (Rrs) and respiratory system elastance (Ers) in comparison to control mice, as has been already shown by Eickmeier et al. [18] (Fig. 5a, g). In our study, the tissue compliance was also significantly diminished in *Atm*-deficient animals ($Atm^{-/-}$ 0.0249 cmH_2O/mL ± 0.0015, $Atm^{+/+}$ 0.0283 cmH_2O/mL ± 0.0016, P < 0.05) (Fig. 5d).

Nine days after BLM treatment, the compliance ($Atm^{-/-}$ 0.0192 cmH_2O/mL ± 0.0075, P < 0.05; $Atm^{+/+}$ 0.0195 cmH_2O/mL ± 0.0067, P < 0.05) significantly decreased, whereas resistance (day 0: $Atm^{-/-}$ 0.909 cmH_2O*s/mL ± 0.031; $Atm^{+/+}$ 0.638 cmH_2O*s/mL ± 0.021, day 9: $Atm^{-/-}$ 1.073 cmH_2O*s/mL ± 0.095; $Atm^{+/+}$ 0.922 cmH_2O*s/mL ± 0.035, P < 0.01) and elastance (day 0: $Atm^{-/-}$ 39.21 cmH_2O*s/mL ± 0.172; $Atm^{+/+}$ 32.68 cmH_2O*s/mL ± 0.153, day 9: $Atm^{-/-}$ 54.56 cmH_2O*s/mL ± 0.55; $Atm^{+/+}$ 48.54 cmH_2O*s/mL ± 0.32, P < 0.01) increased in *Atm*-deficient and wild-type mice compared to baseline values (day 0, Fig. 5b, e, h).

Interestingly, 28 days after BLM instillation, the resistance, compliance and elastance did not improve in *Atm*-deficient mice, whereas the compliance did improve in wild-type mice (0.0236 cmH_2O/mL ± 0.0185, P < 0.05). In addition, the resistance ($Atm^{-/-}$ 1.108 cmH_2O*s/mL ± 0.137, $Atm^{+/+}$ 0.735 cmH_2O*s/mL ± 0.088) and elastance ($Atm^{-/-}$ 47.239 cmH_2O*s/mL ± 0.632, $Atm^{+/+}$ 39.579 cmH2O*s/mL ± 0.628) were found to be lower in wild-type than in *Atm*-deficient mice, pointing to irreversible changes in the lung structure of these mice after BLM treatment (Fig. 5c, f, i).

It is important to note that due to their poor physical constitution, approximately 50% of *Atm*-deficient mice belonging to the 28-day observation group died under anaesthesia before lung function measurements could be performed (data not shown).

3.8. BLM treatment induces enhanced oxidative stress and DNA damage in ATM-deficient alveolar epithelial cells

Treatment with increasing BLM concentrations exhibited a dose-dependent decrease in the cell viability of A549 cells (Fig. 6a, b) and in primary lung epithelial cells derived from *Atm*-deficient and wild-type mice (Supplementary Fig. 1 a). After co-incubation with KU55933, an ATM-kinase inhibitor, A549 cells showed a significantly lower viability compared to untreated A549 cells (Fig. 6b).

In addition, we tested KU55933 and 100 mU BLM in relation to the release of intracellular ROS in A549 cells (Fig. 6c, Supplementary Fig. 2 d–f). The flow cytometric analyses revealed a significant increase in DCF signal in A549 cells treated with KU55933 and 100 mU BLM compared to BLM-treated A549 cells without KU55933 and BLM-untreated A549 cells with KU55933 (A549 + BLM + KU55933 1.333 ± 0.054, A549 + BLM 1.183 ± 0.064, A549 + KU55933 1.152 ± 0.037, P < 0.05). This was also true for the BLM treatment of

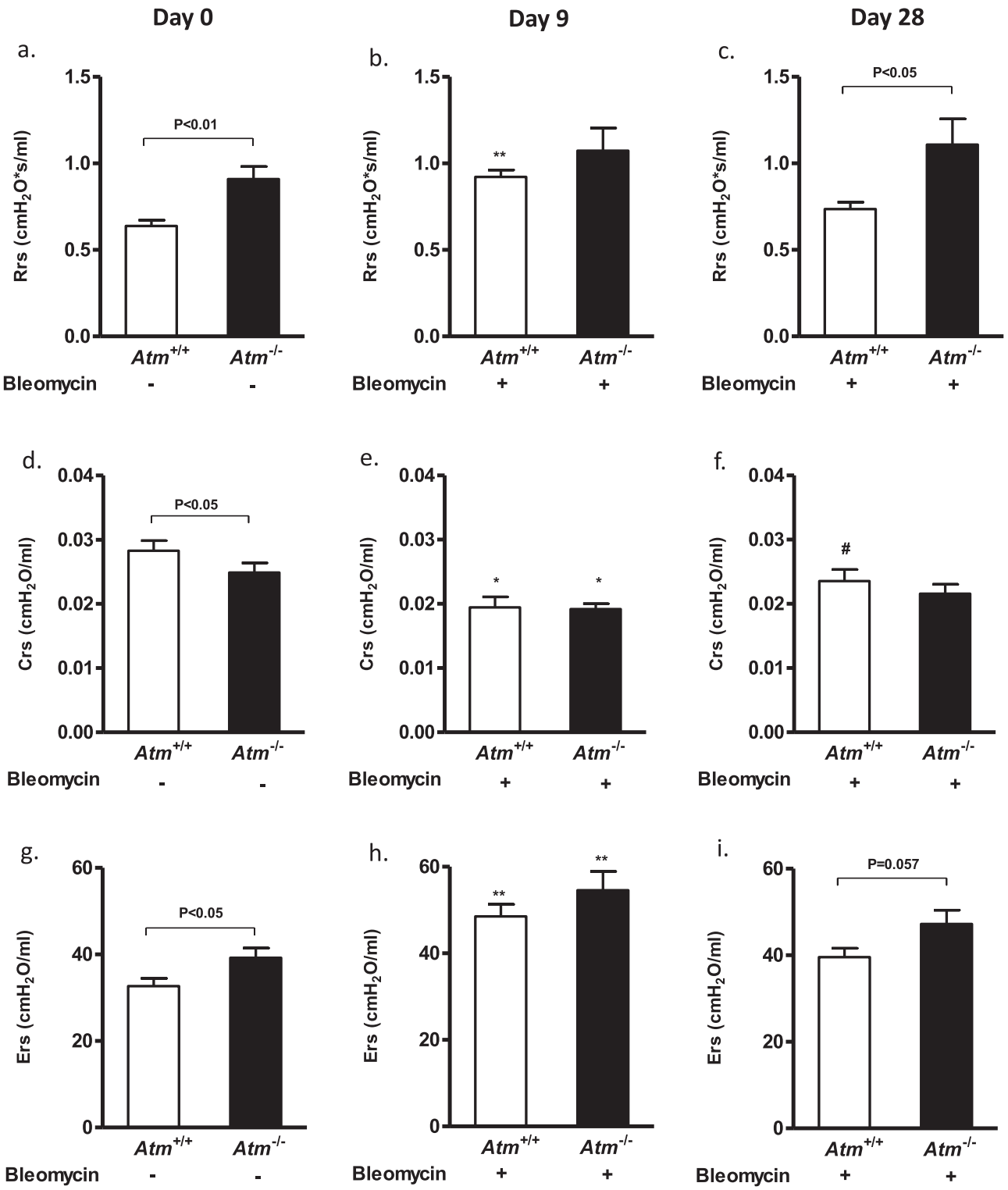

Fig. 5. Using a FlexiVent mouse ventilator, respiratory system (a–c) resistance, (d–f) compliance and (g–i) elastance was determined before (day 0 = baseline, left), 9 days (middle) and 28 days (right) after BLM-induced lung injury in *Atm*$^{-/-}$ mice compared to the *Atm*$^{+/+}$ control group. Values represent the mean ± SEM; day 0 (n = 18), day 9 (n ≥6), day 28 (n ≥ 4). *compared to baseline, # compared *Atm*$^{-/-}$ vs. *Atm*$^{+/+}$, * P < 0.05, ** P < 0.01, # P < 0.05, ## P < 0.01. BLM = bleomycin.

Atm-deficient primary lung epithelial cells (Supplementary Fig. 2 b). DCF fluorescence was significantly increased in untreated lung cells from *Atm*-deficient mice relative to stimulation with 10 mU BLM (Fold increase in *Atm*$^{-/-}$ mice 1.08 ± 0.02 relative to untreated, P < 0.05).

BLM treatment induced DNA-damage in A549 cells irrespective of the presence of ATM as measured by Comet assay (Fig. 6d, e). As it is well described in the literature, BLM-induced double-strand breaks (DSBs) result in the phosphorylation of the histone γH2AX [28,29]. Fig. 6f shows representative γH2AX immuno-stained images of A549 cells before and 3 h after 100 mU BLM stimulation. BLM treatment resulted in a significant increase of the γH2AX signal compared to untreated A549 cells regardless of the presence of the ATM-kinase inhibitor KU55933 (Fig. 6f and Supplementary Fig. 2g). In contrast, BLM-treated A549 cells showed a time-dependent delay in the resolution of

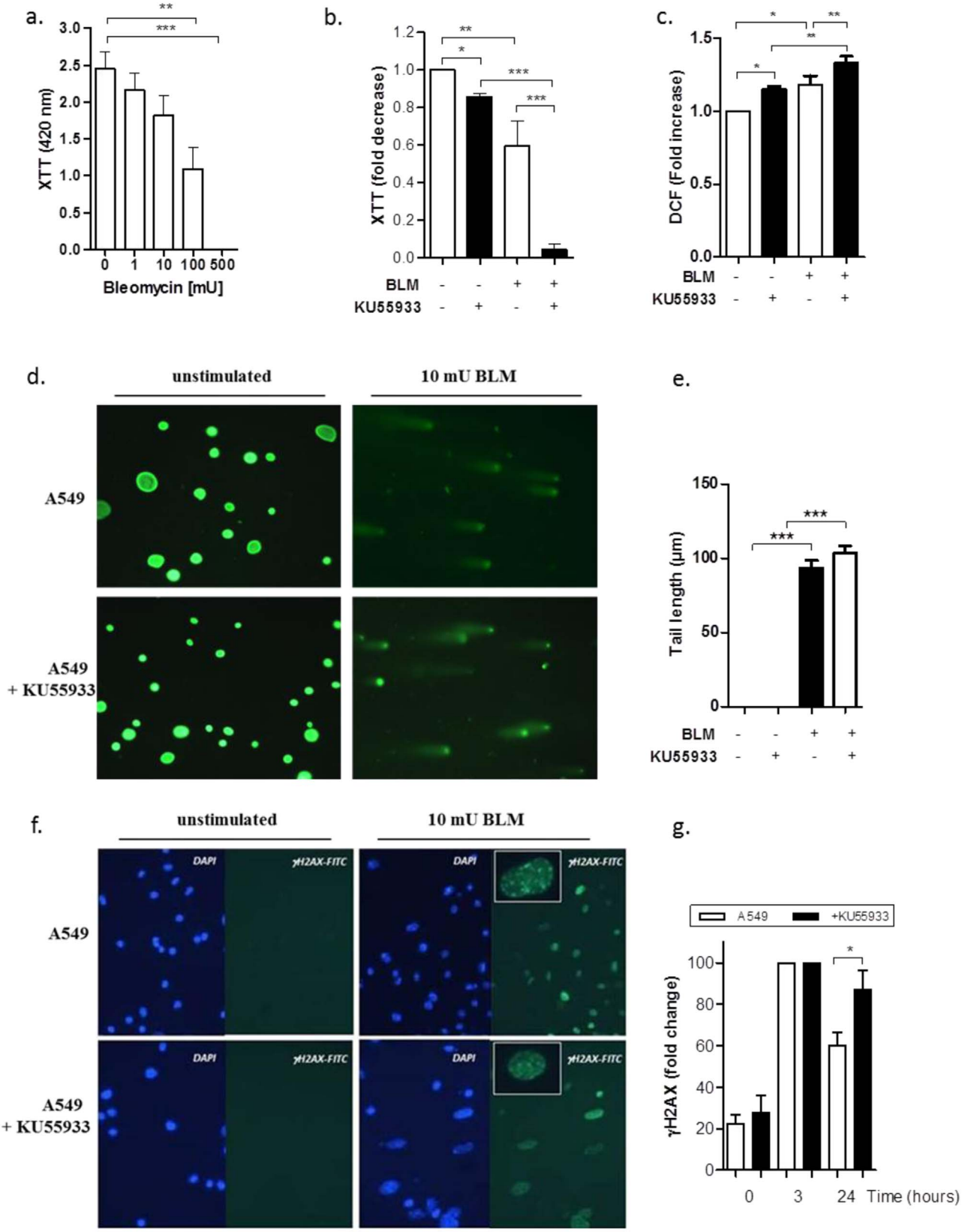

Fig. 6. Effect of BLM on cell viability, oxidative stress and DNA damage on human adenocarcinomic alveolar basal epithelial cells (A549 cell line) *in vitro*. (a) XTT proliferation analysis of A549 cells treated with different BLM concentrations (1 mU, 10 mU, 100 mU and 500 mU; n ≥ 7) (b) XTT proliferation assay of A549 cells in the presence or absence of the ATM-kinase inhibitor KU55933 and treated with or without 100 mU BLM for 24 h (n ≥ 5). (c) Quantitative analysis of ROS levels in the presence or absence of 100 mU BLM and KU55933 in A549 cells measuring DCF uptake in FACS. (d) Representative microscopic appearances of comet assay. A549 cells were treated with or without 10 mU BLM in the presence or absence of KU55933. (e) Neutral comet assay showing DNA double-strand breaks measured by tail length (µm) after 3 h treatment of A549 cells with or without BLM (10 mU) and KU55933 (10 µM). (f) Representative γH2AX (green) and DAPI (blue) immuno-stained images for A549 cells before and 3 h after 100 mU BLM stimulation. Images shown at ×40 magnification. (g) Functionality of A549 cells in the presence or absence of KU55933, as evidenced by their DNA DSB repair capacity using the γH2AX assay (n ≥ 5) over the time. Data are shown as the mean ± SEM. * $P < 0.05$; ** $P < 0.01$; *** $P < 0.001$. BLM = bleomycin, DCF = 2′,7′ –dichlorofluorescein diacetate, DSB = double-strand break, ROS = reactive oxygen species.

γH2AX expression in the presence of KU55933 (after 24 h: A549 46.80 ± 4.76; A549 + KU55933 71.20 ± 7.88; $P < 0.05$) (Fig. 6g, Supplementary Fig. 2h). This decelerated γH2AX resolution was also seen in *Atm*-deficient primary lung epithelial cells (Supplementary Fig. 2 c).

4. Discussion

One of the characteristic features of A-T is recurrent and chronic respiratory disease leading to substantial morbidity and mortality. Several factors have been described to underlie the increased susceptibility to chronic lung disease, including abnormal injury repair, systemic inflammation and oxidative stress. In addition, recurrent sinopulmonary infections, immunodeficiency, aspiration from dysfunctional swallowing due to neurodegenerative progression and respiratory muscle weakness may contribute to the development of lung disease [6]. Lung disease in A-T develops over time, and many of the patients are confronted with bronchiectasis, chronic inflammation and pulmonary fibrosis in the second decade of life. The underlying mechanism is not fully understood yet, and progression is difficult to model, but impaired DNA damage recognition and repair and sensitivity to ROS have to be considered causal factors for respiratory disease in A-T. To investigate bronchoalveolar sensitivity to ROS and ROS-induced DNA damage in A-T, we used BLM to induce experimental inflammation and fibrotic changes in the *Atm*-deficient mouse model [30]. Oropharyngeal BLM administration resulted in a tremendous increase in lung inflammation, fibrosis and irreversible lung function changes in *Atm*-deficient mice.

In patients with A-T, ongoing low-grade inflammation has been described together with altered lung function parameters [7,8]. In the *Atm*-deficient mouse model, we did not find intrinsic inflammation in the lung, confirming previous data from Eickmeier et al. who found slightly restricted lung function in *Atm*-deficient mice without any signs of ongoing inflammation [18]. Considering that the mice have been kept in individually ventilated cages, one reason could be that they have not been in contact with harmful microorganisms, which is an exogenous source that triggers inflammation. Another reason that lung problems are rarely found in the *Atm*-deficient mouse model is probably because the animals die from thymic tumours before lung disease can develop.

However, as it has been shown by Eickmeier et al., *Atm*-deficient mice displayed altered lung function parameters and disrupted immunoregulation after airway mucosal damage [18]. In addition, by characterising primary lung cell populations from *Atm*-deficient mice we showed an increased percentage of alveolar epithelial type 2 cells (AEC2) accompanied by elevated fibroblasts compared to wild-type mice. Despite their function in secretion of surfactant, AEC2 serve as a reservoir of cells that cover damaged lung epithelial cells and, together with an increase in fibroblasts, point to an early stage of tissue remodelling [31]. In our experiments, we also found that ROS levels were elevated in lung cells from *Atm*-deficient mice, especially in the AEC2 population. This result is not surprising and is in line with previous findings of higher levels of 8-hydroxy-2′-deoxyguanosine concentrations in the lung of *Atm*-deficient mice compared to wild-type mice, pointing to increased oxidative stress and damage in the A-T lung [9,32]. On the other hand it was surprising that we haven't seen changes in ROS in fibroblasts of *Atm*-deficient lungs and we only can speculate about the reason. One possible explanation might be that the higher basal levels of oxidative stress that we found in the Sca-1^+ and CD326 cell population cover the DCF-signal in *Atm*-deficient fibroblasts.

Disturbances in redox balance are described for a variety of airway diseases, such as asthma, chronic obstructive pulmonary disease, idiopathic pulmonary fibrosis and lung cancer [33]. Moreover, endogenous and exogenous ROS are central to the progression of many inflammatory disorders and play a significant role in tissue fibrogenesis [34]. While the major sources of endogenous ROS responsible for inflammation are generated in the mitochondria via oxidative phosphorylation, the main sources of exogenous ROS are microbial and viral infections or exposure to radiation and toxic substances [35]. In this regard, loss of mitochondrial integrity connected to oxidative stress and damage have already been shown in *Atm*-deficient mice [16].

A recent report demonstrated that *Streptococcus pneumoniae*, a common organism of the upper respiratory tract that is implicated in sinopulmonary infections in A-T patients, caused DNA double-strand breaks and apoptosis in epithelial cells by secreting H_2O_2, an agent known to cause oxidative stress [36]. Moreover, Yeo et al. demonstrated the susceptibility of AECs from A-T patients to oxidative stress [37].

Based on these observations and our recent findings, we predict that A-T AECs will be particularly sensitive to endogenous and exogenous ROS and that the underlying mechanism of lung disease in A-T might be an accumulation of oxidative stress and damage over time that leads to lung tissue damage.

Chronic, crippling lung disease in A-T patients develops over time, and the monitoring disease progression is difficult to implement in these patients [5]. Major reasons for monitoring difficulty are the following: Due to the high sensitivity to ionizing radiation, repeated X-rays and CT scans should be avoided; Current MRI sequences are limiting; performing a valid spirometry is challenging due to neurological difficulties. Therefore, we have established the BLM model *in vivo* in the *Atm*-deficient mouse to follow the progression of inflammatory and fibrotic changes in pulmonary tissue, as well as changes in the lung. BLM administration resulted in a tremendous increase in lung inflammation and fibrotic changes in the lung tissue of *Atm*-deficient mice, accompanied by significant deterioration of lung function. Interestingly, lung function testing revealed an irreversible change in lung resistance, elastance and compliance after BLM treatment. This was also reflected in weight loss, which never fully recovered.

The data are in line with pulmonary function testing in older A-T patients, showing a mixed pattern of obstructive and restrictive lung disease [3,38]. Like the untreated *Atm*-deficient mice that showed decreased compliance and increased obstruction, Montella et al. [39] demonstrated early structural changes, such as bronchiectasis and consolidation, in the lungs of A-T patients using high-field magnetic resonance imaging (MRI). Following this line of reasoning, low-grade inflammation associated with lower lung function could be another indication of changes in the lung homeostasis of A-T patients [8].

Given the observed increased inflammation, which resulted in strong fibrotic changes and irreversible tissue damage, our findings demonstrate a very high sensitivity to and low protection of A-T lungs against ROS and ROS-inducing DNA damaging agents, suggesting a role of ATM for epithelial cell integrity and homeostasis. BLM treatment of isolated primary AEC2 from *Atm*-deficient mice and of the human epithelial cell line A549 with the ATM-kinase inhibitor KU55933 confirmed this hypothesis. ATM-deficiency in AEC2 caused significantly reduced cell viability after BLM treatment compared to ATM-competent cells and a delay in the resolution of γH2AX-expression [40]. However, more importantly, ATM deficiency led to an increase in spontaneous intracellular ROS, which was significantly increased after BLM treatment.

Recent data show the cytotoxic and mutagenic effects of bleomycin on epithelial cells and confirm the role of ATM in the adequate functioning of the DNA-repair pathway in response to BLM-induced DNA damage [40,41]. High levels of ROS after exposure to BLM were also shown in Nijmegen Breakage Syndrome (NBS), another genetic instability syndrome [42]. Furthermore, Guo et al. recently demonstrated that ROS induces ATM activation in the absence of DNA double-strand breaks [43]. This finding is of great importance because of the crucial role of ROS in A-T. Many groups, including ours, have demonstrated that the loss of ATM is connected to increased concentrations of ROS and hypersensitivity to agents that induce oxidative stress in various

cells and tissues [13,16,44]. In this regard, sensitivity to ROS in lung epithelial cells is a logical consequence and supports the hypothesis that oxidative stress may contribute to lung disease in A-T.

In conclusion, our results demonstrate high bronchoalveolar sensitivity to ROS and ROS-induced DNA damage in the *Atm*-deficient mouse model that might reflect the clinical course of lung damage in A-T or at least the progression of interstitial lung disease and fibrosis [4]. The BLM animal model could be a useful tool to investigate potential treatment options to test compounds, such as antioxidants or the use of mesenchymal stromal cells, for their capacity to counteract pulmonary disease in A-T. Illuminating the origin of A-T lung disease and its progression may help with the discovery and development of therapeutic interventions.

The authors declare no conflict of interest.

Appendix A. Supplementary material

Supplementary data associated with this article can be found in the online version at http://dx.doi.org/10.1016/j.redox.2017.11.006.

References

[1] E. BODER, R.P. SEDGWICK, Ataxia-telangiectasia; a familial syndrome of progressive cerebellar ataxia, oculocutaneous telangiectasia and frequent pulmonary infection, Pediatrics 21 (4) (1958) 526–554.

[2] R.A. Gatti, S. Becker-Catania, H.H. Chun, et al., The pathogenesis of ataxia-telangiectasia. learning from a Rosetta stone, Clin. Rev. Allergy Immunol. 20 (1) (2001) 87–108, http://dx.doi.org/10.1385/CRIAI:20:1:87.

[3] S.A. Schroeder, S. Zielen, Infections of the respiratory system in patients with ataxia-telangiectasia, Pediatr. Pulmonol. 49 (4) (2014) 389–399, http://dx.doi.org/10.1002/ppul.22817.

[4] S.A. Schroeder, M. Swift, C. Sandoval, C. Langston, Interstitial lung disease in patients with ataxia-telangiectasia, Pediatr. Pulmonol. 39 (6) (2005) 537–543, http://dx.doi.org/10.1002/ppul.20209.

[5] S.A. McGrath-Morrow, W.A. Gower, C. Rothblum-Oviatt, et al., Evaluation and management of pulmonary disease in ataxia-telangiectasia, Pediatr. Pulmonol. 45 (9) (2010) 847–859, http://dx.doi.org/10.1002/ppul.21277.

[6] J.M. Bhatt, A. Bush, M. van Gerven, et al., ERS statement on the multidisciplinary respiratory management of ataxia telangiectasia, Eur. Respir. Rev. 24 (138) (2015) 565–581, http://dx.doi.org/10.1183/16000617.0066-2015.

[7] S.A. McGrath-Morrow, J.M. Collaco, T.O. Crawford, et al., Elevated serum IL-8 levels in ataxia telangiectasia, J. Pediatr. 156 (4) (2010) 682, http://dx.doi.org/10.1016/j.jpeds.2009.12.007.

[8] S.A. McGrath-Morrow, J.M. Collaco, B. Detrick, H.M. Lederman, Serum Interleukin-6 Levels and Pulmonary Function in Ataxia-Telangiectasia, J. Pediatr. 171 (2016) 256, http://dx.doi.org/10.1016/j.jpeds.2016.01.002.

[9] J. Pietzner, B.M. Merscher, P.C. Baer, et al., Low-dose irradiation prior to bone marrow transplantation results in ATM activation and increased lethality in ATM-deficient mice, Bone Marrow Transplant. 51 (4) (2016) 619, http://dx.doi.org/10.1038/bmt.2016.22.

[10] K.L. Moffitt, S.L. Martin, A.M. Jones, et al., Inflammatory and immunological biomarkers are not related to survival in adults with Cystic Fibrosis, J. Cyst. Fibros. 13 (1) (2014) 63–68, http://dx.doi.org/10.1016/j.jcf.2013.06.002.

[11] B. Su, T. Liu, H. Fan, et al., Inflammatory markers and the risk of chronic obstructive pulmonary disease: a systematic review and meta-analysis, PLoS One 11 (4) (2016) e0150586, http://dx.doi.org/10.1371/journal.pone.0150586.

[12] O. Eickmeier, M. Huebner, E. Herrmann, et al., Sputum biomarker profiles in cystic fibrosis (CF) and chronic obstructive pulmonary disease (COPD) and association between pulmonary function, Cytokine 50 (2) (2010) 152–157, http://dx.doi.org/10.1016/j.cyto.2010.02.004.

[13] C. Barlow, S. Hirotsune, R. Paylor, et al., Atm-deficient mice: a paradigm of ataxia telangiectasia, Cell 86 (1) (1996) 159–171.

[14] J. Reichenbach, R. Schubert, C. Schwan, K. Müller, H.J. Böhles, S. Zielen, Antioxidative capacity in patients with ataxia telangiectasia, Clin. Exp. Immunol. 117 (3) (1999) 535–539.

[15] J. Reichenbach, R. Schubert, D. Schindler, K. Müller, H. Böhles, S. Zielen, Elevated oxidative stress in patients with ataxia telangiectasia, Antioxid. Redox Signal. 4 (3) (2002) 465–469, http://dx.doi.org/10.1089/15230860260196254.

[16] R. Schubert, L. Erker, C. Barlow, et al., Cancer chemoprevention by the antioxidant tempol in Atm-deficient mice, Hum. Mol. Genet. 13 (16) (2004) 1793–1802, http://dx.doi.org/10.1093/hmg/ddh189.

[17] N. Gueven, J. Luff, C. Peng, K. Hosokawa, S.E. Bottle, M.F. Lavin, Dramatic extension of tumor latency and correction of neurobehavioral phenotype in Atm-mutant mice with a nitroxide antioxidant, Free Radic. Biol. Med. 41 (6) (2006) 992–1000, http://dx.doi.org/10.1016/j.freeradbiomed.2006.06.018.

[18] O. Eickmeier, S.Y. Kim, E. Herrmann, et al., Altered mucosal immune response after acute lung injury in a murine model of Ataxia Telangiectasia, BMC Pulm. Med. 14 (2014) 93, http://dx.doi.org/10.1186/1471-2466-14-93.

[19] A. Moeller, K. Ask, D. Warburton, J. Gauldie, M. Kolb, The bleomycin animal model: a useful tool to investigate treatment options for idiopathic pulmonary fibrosis? Int. J. Biochem Cell Biol. 40 (3) (2008) 362–382, http://dx.doi.org/10.1016/j.biocel.2007.08.011.

[20] I.Y. Adamson, Pulmonary toxicity of bleomycin, Environ. Health Perspect. 16 (1976) 119–126.

[21] H. Umezawa, M. Ishizuka, K. Maeda, T. Takeuchi, Studies on bleomycin, Cancer 20 (5) (1967) 891–895.

[22] C.A. Claussen, E.C. Long, Nucleic acid recognition by metal complexes of bleomycin, Chem. Rev. 99 (9) (1999) 2797–2816.

[23] V. Vooght, J.A.J. de, Vanoirbeek, S. Haenen, E. Verbeken, B. Nemery, P.H.M. Hoet, Oropharyngeal aspiration: an alternative route for challenging in a mouse model of chemical-induced asthma, Toxicology 259 (1–2) (2009) 84–89, http://dx.doi.org/10.1016/j.tox.2009.02.007.

[24] M. Lieber, B. Smith, A. Szakal, W. Nelson-Rees, G. Todaro, A continuous tumor-cell line from a human lung carcinoma with properties of type II alveolar epithelial cells, Int. J. Cancer 17 (1) (1976) 62–70.

[25] M. Corti, A.R. Brody, J.H. Harrison, Isolation and primary culture of murine alveolar type II cells, Am. J. Respir. Cell Mol. Biol. 14 (4) (1996) 309–315, http://dx.doi.org/10.1165/ajrcmb.14.4.8600933.

[26] T. Tanaka, D. Halicka, F. Traganos, Z. Darzynkiewicz, Cytometric analysis of DNA damage: phosphorylation of histone H2AX as a marker of DNA double-strand breaks (DSBs), Methods Mol. Biol. 523 (2009) 161–168, http://dx.doi.org/10.1007/978-1-59745-190-1_11.

[27] T. Ashcroft, J.M. Simpson, V. Timbrell, Simple method of estimating severity of pulmonary fibrosis on a numerical scale, J. Clin. Pathol. 41 (4) (1988) 467–470.

[28] S. Burma, B.P. Chen, M. Murphy, A. Kurimasa, D.J. Chen, ATM phosphorylates histone H2AX in response to DNA double-strand breaks, J. Biol. Chem. 276 (45) (2001) 42462–42467, http://dx.doi.org/10.1074/jbc.C100466200.

[29] C.E. Rübe, S. Grudzenski, M. Kühne, et al., DNA double-strand break repair of blood lymphocytes and normal tissues analysed in a preclinical mouse model: Implications for radiosensitivity testing, Clin. Cancer Res. 14 (20) (2008) 6546–6555, http://dx.doi.org/10.1158/1078-0432.CCR-07-5147.

[30] V. Della Latta, A. Cecchettini, S. Del Ry, M.A. Morales, Bleomycin in the setting of lung fibrosis induction: from biological mechanisms to counteractions, Pharmacol. Res. 97 (2015) 122–130, http://dx.doi.org/10.1016/j.phrs.2015.04.012.

[31] H. Fehrenbach, Alveolar epithelial type II cell: defender of the alveolus revisited, Respir. Res. 2 (1) (2001) 33–46.

[32] R. Reliene, E. Fischer, R.H. Schiestl, Effect of N-acetyl cysteine on oxidative DNA damage and the frequency of DNA deletions in atm-deficient mice, Cancer Res. 64 (15) (2004) 5148–5153, http://dx.doi.org/10.1158/0008-5472.CAN-04-0442.

[33] I. Rahman, S.K. Biswas, A. Kode, Oxidant and antioxidant balance in the airways and airway diseases, Eur. J. Pharmacol. 533 (1–3) (2006) 222–239, http://dx.doi.org/10.1016/j.ejphar.2005.12.087.

[34] M. Mittal, M.R. Siddiqui, K. Tran, S.P. Reddy, A.B. Malik, Reactive oxygen species in inflammation and tissue injury, Antioxid. Redox Signal. 20 (7) (2014) 1126–1167, http://dx.doi.org/10.1089/ars.2012.5149.

[35] P. Di Rosanna, C. Salvatore, Reactive oxygen species, inflammation, and lung diseases, Curr. Pharm. Des. 18 (26) (2012) 3889–3900.

[36] P. Rai, M. Parrish, I.J.J. Tay, et al., Streptococcus pneumoniae secretes hydrogen peroxide leading to DNA damage and apoptosis in lung cells, Proc. Natl. Acad. Sci. USA 112 (26) (2015) 30, http://dx.doi.org/10.1073/pnas.1424144112.

[37] A.J. Yeo, E. Fantino, D. Czovek, C.E. Wainwright, P.D. Sly, M.F. Lavin, Loss of ATM in Airway Epithelial Cells Is Associated with Susceptibility to Oxidative Stress, Am. J. Respir. Crit. Care Med. 196 (3) (2017) 391–393, http://dx.doi.org/10.1164/rccm.201611-2210LE.

[38] S.A. McGrath-Morrow, H.M. Lederman, A.D. Aherrera, et al., Pulmonary function in children and young adults with ataxia telangiectasia, Pediatr. Pulmonol. 49 (1) (2014) 84–90, http://dx.doi.org/10.1002/ppul.22760.

[39] S. Montella, C. Mollica, A. Finocchi, et al., Non invasive assessment of lung disease in ataxia telangiectasia by high-field magnetic resonance imaging, J. Clin. Immunol. 33 (7) (2013) 1185–1191, http://dx.doi.org/10.1007/s10875-013-9933-y.

[40] T. Allio, R.J. Preston, Increased sensitivity to chromatid aberration induction by bleomycin and neocarzinostatin results from alterations in a DNA damage response pathway, Mutat. Res. 453 (1) (2000) 5–15.

[41] A. Elson, Y. Wang, C.J. Daugherty, et al., Pleiotropic defects in ataxia-telangiectasia protein-deficient mice, Proc. Natl. Acad. Sci. USA 93 (23) (1996) 13084–13089.

[42] H. Krenzlin, I. Demuth, B. Salewsky, et al., DNA damage in Nijmegen Breakage Syndrome cells leads to PARP hyperactivation and increased oxidative stress, PLoS Genet. 8 (3) (2012) e1002557, http://dx.doi.org/10.1371/journal.pgen.1002557.

[43] Z. Guo, S. Kozlov, M.F. Lavin, M.D. Person, T.T. Paull, ATM activation by oxidative stress, Science 330 (6003) (2010) 517–521, http://dx.doi.org/10.1126/science.1192912.

[44] K. Ito, K. Takubo, F. Arai, et al., Regulation of reactive oxygen species by Atm is essential for proper response to DNA double-strand breaks in lymphocytes, J. Immunol. 178 (1) (2007) 103–110.